Journal of Inorganic and Organometallic Polymers and Materials (2020) 30:2626–2632
https://doi.org/10.1007/s10904-020-01460-6

One Step Synthesis and Characterization of ZnO–ZnSe Heterostructures by Chemical Precipitation and Its Solar Photocatalytic Activity

Lakshmi Mohan[1,4] · Nila Sisupalan[1] · Kathirvel Ponnusamy[2] · Saravanakumar Sadagopalan[3]

Received: 25 October 2019 / Accepted: 28 January 2020 / Published online: 1 February 2020

Abstract
ZnO–ZnSe heterostructures were successfully synthesized by single step chemical precipitation method at room temperature. The obtained composite structures were systematically characterized for structural, morphological, optical, and vibrational properties using X-ray diffraction (XRD), field emission scanning electron microscope (FESEM), High-resolution transmission electron microscopy (HRTEM), UV–Vis DRS, photoluminescence spectroscopy (PL), and Fourier-transform Raman spectroscopy (FT-Raman). XRD patterns of the synthesized samples exhibit peaks corresponding to wurtzite ZnO and ZnSe structures which primarily confirmed the formation of single phase heterostructures. ZnO microspheres grown over the surface of ZnSe nano cauliflower clusters obtained from the FESEM images confirmed the formation of ZnO–ZnSe heterostructures. A sharp peak around 290 nm in UV–Vis DRS absorption spectra corresponds to $ZnSeO_3$ and a wide weak absorbance is observed in the visible region (ranging from 370 to 663 nm) corresponding to the nanocomposite structure. In the Raman spectra, the surface phonon mode which is the characteristic feature of the ZnO–ZnSe heterostructures is observed at 237 cm^{-1}. Based on the characterization results, the photocatalytic properties of ZnO–ZnSe nanoparticles were evaluated for the degradation of methylene blue (MB) and was found to exhibit solar photocatalytic property.

Keywords ZnO–ZnSe heterostructures · Wurtzite structure · Chemical precipitation method · Photocatalytic degradation

1 Introduction

Nanostructured materials have gained more significance in the recent past owing to its dependence on the optical and electrical properties with morphology [1]. With the appropriate choice of materials, metal /semiconductors nanostructures can modify the optical and catalytical properties. They equally gain importance as they are environmentally safe [2, 3]. Zinc oxide (ZnO), one among metal-oxide semiconductors exhibits these properties. The intrinsic properties of ZnO nanostructures can be tuned by doping or developing heterostructures or nanocomposites with suitable materials [4, 5]. Being a wide bandgap semiconductor, absorption of light in the visible range is not feasible using ZnO nanostructures (bandgap 3.37 eV). The volant recombination of charge carriers is another hindrance for not utilizing ZnO for photocatalytic applications to the fullest. Nanocomposites or heterostructures with ZnO can improve charge separation and photo response [6]. Zinc selenide (ZnSe), another wide bandgap semiconductor is a metal chalcogenide with 1:1 stoichiometry having a wide range of optical and catalytical properties. The bandgap of ZnSe (2.67 eV) is smaller compared with ZnO, hence ZnSe is a desirable material to synthesize heterostructures along with ZnO, as it can enhance the charge separation also [7–9]. Various routes for synthesizing of ZnO–ZnSe heterostructures have already been reported [10–13]. In this report we detail about the synthesis of ZnO–ZnSe heterostructure nanoparticles using chemical precipitation method and investigate the structural,

✉ Lakshmi Mohan
lakshmi_mohan@cb.amrita.edu

[1] Department of Sciences, Amrita School of Engineering, Coimbatore, Amrita Vishwa Vidyapeetham, India

[2] GRD Centre for Materials Research, Department of Physics, PSG College of Technology, Coimbatore, Tamil Nadu 641004, India

[3] Department of Physics, N S S College, Pandalam, Kerala 689501, India

[4] Research and Development Center, Bharathiar University, Coimbatore, Tamil Nadu 641046, India

optical, morphological, vibrational properties thus leading to the photocatalytic degradation property which is confirmed with methylene blue (MB).

2 Materials and Methods

2.1 Chemicals

Zinc acetate dihydrate [$Zn(CH_3COO)_2{\cdot}2H_2O$] (Merck), Polyvinyl pyrrolidone [PVP] (Hi media), Sodium Selenite pentahydrate [$Na_2SeO_3{\cdot}5H_2O$] (Research-lab fine), Ethylene glycol monobutyl ether [$C_6H_{14}O_2$] (Research-lab fine), Hydrazine hydrate [$N_2H_4{\cdot}H_2O$] (Research-lab fine), Methylene blue [$C_{16}H_{18}CIN_3S$] (Hi media). All the chemicals used were of AR grade and used without further purification. Deionized water was used in all the experiments.

2.2 Synthesis

Various routes for synthesizing of ZnO/ZnSe heterostructures have already been reported. The one-step synthesis of PVP coated ZnO/ZnSe nanostructures by chemical precipitation is as follows. Initially, the required amount of PVP and 0.2 M $Na_2SeO_3{\cdot}5H_2O$ were added to 25 ml, 0.2 M $Zn(CH_3COO)_2{\cdot}2H_2O$ under vigorous stirring followed by the addition of an equal ratio (1:1) of $N_2H_4{\cdot}H_2O$ and $C_6H_{14}O_2$. The resultant solution was continuously stirred for 7 h. The neon coral orange colored precipitate obtained was filtered, washed, and dried, followed by annealing at 200 °C for 3 h.

2.3 Characterization Techniques

Different characterization techniques were used to investigate the structural, morphological, optical, and functional properties. In this work, the structural analysis of the prepared samples were recorded using XRD Philip PW1700 (wavelength 1.54 Å, 40 kV 40 mA) in 2θ geometry in the range of 25°–65°. The field emission scanning electron microscope (FESEM) and energy dispersive X-ray analysis (EDX) is used to study the surface morphology and elemental composition of the synthesized samples using Carl Zeiss. Jeol/JEM 2100 system was used for High-resolution transmission electron microscopy (HRTEM) measurements using LaB_6 as the source and was operated at 200 kV. To study the optical reflectance and absorbance properties, UV–Vis diffused reflectance spectra was recorded in the wavelength range of 250–800 nm at room temperature, using JASCO UV–Vis NIR spectrometer (model name; V-670). The Photoluminescence (PL) studies were performed using a JASCO FLUOROSCENCE spectrum (model name; FP-8300) with Xenon lamp at an excitation wavelength of 300 nm. Raman spectra of the sample was recorded in the range 100–600 cm^{-1} using BRUKER RFS 27.

2.4 Photocatalytic Studies

The solar photocatalytic activity of the synthesized sample was evaluated by estimating the photocatalytic degradation of Methylene blue in water 0.10 mg of the synthesized sample is dispersed in 100 ml of MB solution (10 mg l^{-1}) and was continuously stirred for 30 min in dark, to ensure adsorption–desorption equilibrium. These samples were irradiated with sunlight for 210 min (3.5 h). At every 30 min interval, the absorbance of the sample was noted. A partial dose of the solution was extracted and centrifuged to remove the photocatalyst to measure the absorbance using a UV–Vis spectrophotometer. The maximum absorbance of MB is centered around 664 nm (Fig. 9) [14, 15].

3 Results and Discussion

3.1 X-Ray Diffraction Analysis (XRD)

Figure 1 represents the X-ray diffraction pattern of the synthesized samples The patterns exhibits peaks corresponding to wurtzite ZnSe structure which is in well agreement with the JCPDS card data (80-0008) and three standard peaks at 31.79°, 34.42°, 36.25° corresponding to hexagonal wurtzite structure of ZnO was observed which was also corroborated with the JCPDS card data (36-145).Two additional peaks at 35.57° and 43.34° correspond to orthorhombic Zinc Selenite ($ZnSeO_3$) (JCPDS card no: 01-089-2940). No other impurity peaks were detected, there by indicating the possibility

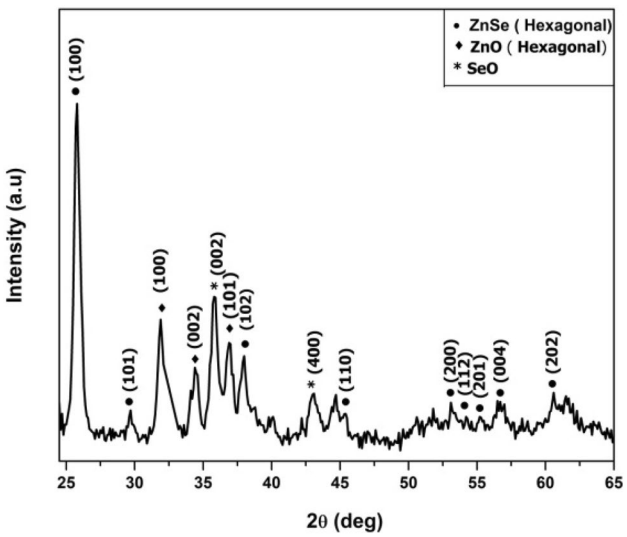

Fig. 1 XRD diffractogram of ZnO–ZnSe heterostructure

of formation of heterostructures. Synthesis of ZnO/ZnSe wurtzite heterostructures were not reported much using chemical co-precipitation method at room temperature. The suggested reaction mechanism for this case can be explained as follows:

The dissociation of Zinc acetate in the solution gives rise to Zn^{2+} ions in the solution onto which PVP is added. PVP serves as a surfactant in the reaction. Dissociation of $Na_2SeO_3{\cdot}5H_2O$ gives SeO_3^{2-} ions in the solution. Ethylene glycol along with hydrazine hydrate acts as reducing agent and reduces SeO_3^{2-} into Se. The unreduced SeO_3^{2} combines with Zn^{2+} to form $ZnSeO_3$ [16–19]. The reaction can be represented as follows

$$SeO_3^{2-} + H_6N_2O \rightarrow Se + N_2 + OH^- + 2H_2O \quad (1)$$

$$Zn^{2+} + Se + OH^- + \underset{\text{(unreduced)}}{SeO_3^{2}} \rightarrow ZnSe + ZnOH + ZnSeO_3 \quad (2)$$

On drying the sample followed by annealing ZnOH gets converted to ZnO.

The crystalline size was calculated for the (100) peak using Debye Scherrer formula [18].

$$(D = K\lambda/\beta\cos\theta) \quad (3)$$

The wurtzite lattice parameters like the interplanar spacing (d) [5] lattice constants (a) and (c), bondlength (L) and volume (V) are calculated using the following equations (Eqs. 4–7) [20, 21] and the values are summarized in Table 1.

For hexagonal wurtzite structure, a = b ≠ c;

$$\frac{1}{d^2} = \frac{4}{3}\left(\frac{h^2 + hk + k^2}{a^2}\right) + \left(\frac{l^2}{c^2}\right) \quad (4)$$

$$a = \frac{\lambda}{\sqrt{3}\sin\theta},\ c = \frac{\lambda}{\sin\theta} \quad (5)$$

$$L = \sqrt{\left(\frac{a^2}{2} + \left(\frac{1}{2} - u\right)^2 c^2\right)}, \quad (6)$$

where $u = \frac{a^2}{3c^2} + 0.25$

$$V = \left(a^2\right) * c \quad (7)$$

3.2 Morphological and Elemental Composition Study

3.2.1 Field-Emission Scanning Electron Microscope (FESEM)

Figure 2 shows the FESEM image of the synthesized nanoparticles and from the figure it was observed that ZnO

Table 1 Lattice parameters of PVP/ZnO/ZnSe heterostructure nanoparticles

Sample name	Plane (hkl)	Highest peak (2θ)deg	FWHM (deg)	D (crystalline size) nm	A (A^{θ})	C (A^{θ})	Volume (a^2)*c (nm^3)	Bond length L (nm)
ZP (ZnSe)	100	25.78	0.56	15.03	3.98	6.48	0.08	0.24
ZnO	100	31.90	0.57	14.89	3.23	5.21	0.04	0.19

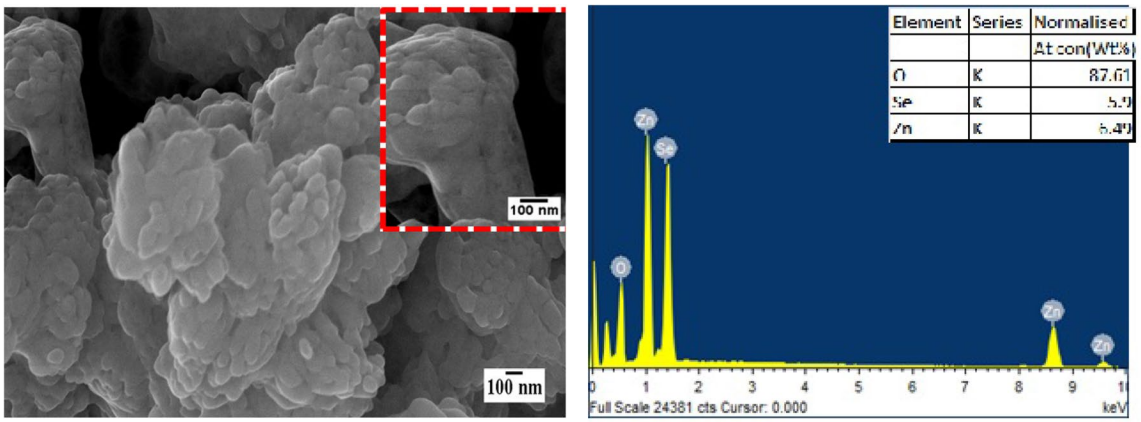

Fig. 2 FESEM micrograph and EDAX spectra of synthesized ZnO–ZnSe heterostructures

microspheres grown over the ZnSe nano cauliflower clusters thus forming a ZnO/ZnSe layered plate structure confirming the ZnO/ZnSe heterostructure. This cauliflower morphology is formed when both the nuclei formation and growth of the nanoparticles occurred simultaneously [22]. The coating of PVP can be distinguished on the higher magnification. The elemental composition of the ZnO–ZnSe heterostructured nanoparticles was determined by energy dispersive X-ray analysis (EDX) analysis which is attached to the FESEM instrument. The existence of Zinc (Zn), Selenium (Se), and Oxygen (O) elements is confirmed from the EDX analysis (inset Fig. 2). Analysis showed Zn and Se element existed with almost 1:1 ratio and composition of oxygen indicates the formation of $ZnSeO_3$ owing to the unreduced SeO_3 which corroborates the XRD results [23, 24].

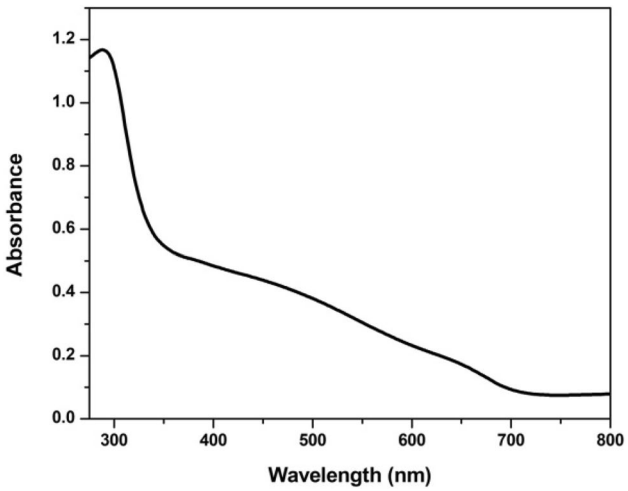

Fig. 4 Absorbance plot of synthesized ZnO–ZnSe heterostructures

3.2.2 High-Resolution Transmission Electron Microscopy (HRTEM)

The synthesized ZnO–ZnSe heterostructures nanoparticles were further characterized using the High-resolution transmission electron microscopy (HRTEM), which is a phase contrast image that gives information on the atomic scale. As it can be seen from the Fig. 3 that the ZnO nanoparticles are approximately spherical in shape, and thus can find similarity from the findings obtained by the FESEM image. The figure also confirms the PVP encapsulation on the outer regions.

3.3 UV–Vis Diffuse Reflectance Spectroscopy (UV–Vis DRS)

The absorbance plot obtained shows absorption in UV as well as in visible region as shown in the Fig. 4. The UV–Vis DRS absorption spectra around 310 nm which corresponds to the characteristic band gap of $ZnSeO_3$ nanocomposites [22]. A broad weak absorbance is observed in the visible region. The visible region absorbance was taken as the key reason in testing photocatalytic activity of the ZnO/ZnSe heterostructures. The ZnO and ZnSe peaks are centred around 370 nm and ZnSe absorption peaks are centered around 470 nm as reported in literatures [4, 25]. Due to the improved visible light absorption of the heterostructures there will be an enhancement in the generation of charged carriers [13]. For this reason there is a possibility that under visible illumination and it can exhibit photocatalytic properties.

The optical direct band gap value was obtained from Tauc plot (Fig. 5) [26, 27]. It is observed that the band-gap energy plot contains single slop only which suggests the direct allowed transition only. Heiba et al. has already reported that unconstrained oxygen occupancy and oxygen diffusion occurs due to the formation of ZnO and $ZnSeO_3$ [28]. This can be ascribed as the reason for the shift of band gaps of the synthesized sample [e.g. 3.94 eV] when

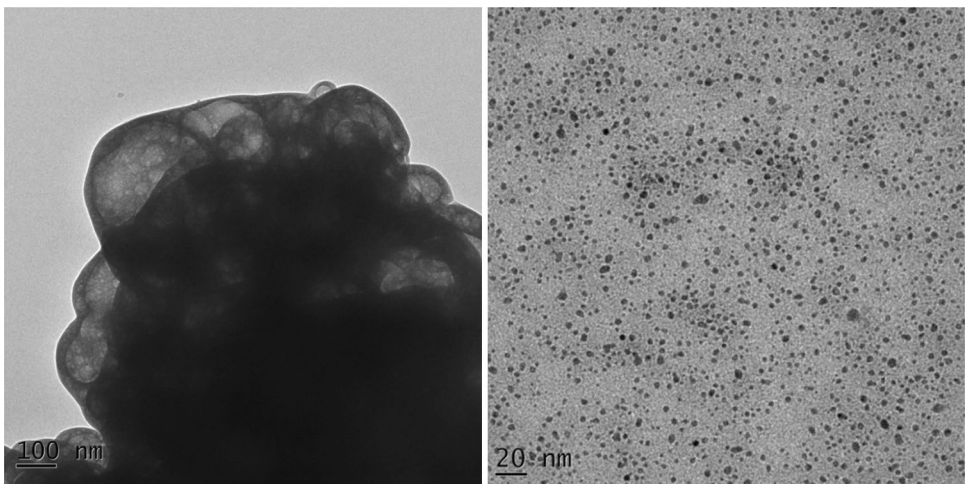

Fig. 3 HRTEM images of synthesized ZnO–ZnSe heterostructures

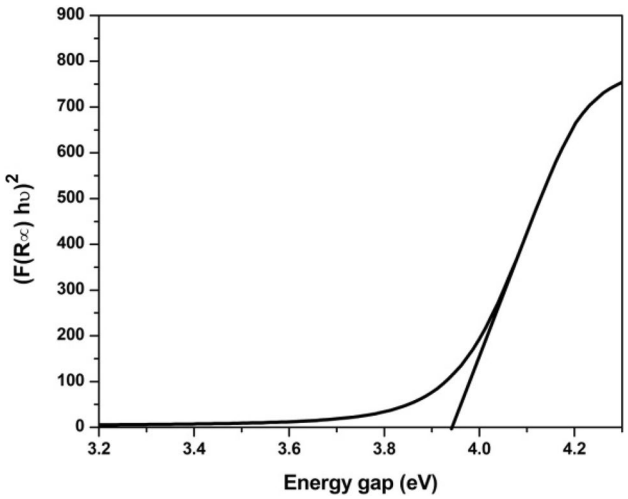

Fig. 5 Tauc plot of synthesized ZnO–ZnSe heterostructures

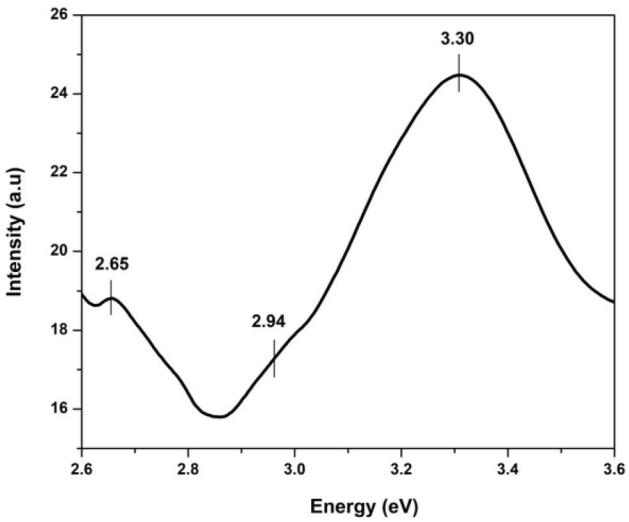

Fig. 7 Energy plot of synthesized ZnO–ZnSe heterostructures

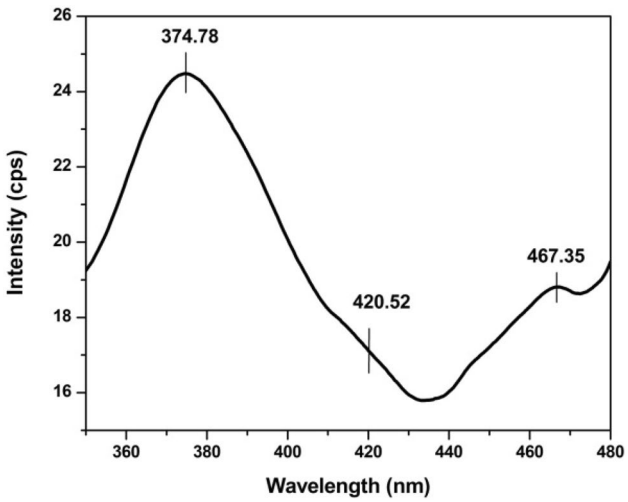

Fig. 6 PL plot of synthesized ZnO–ZnSe heterostructures

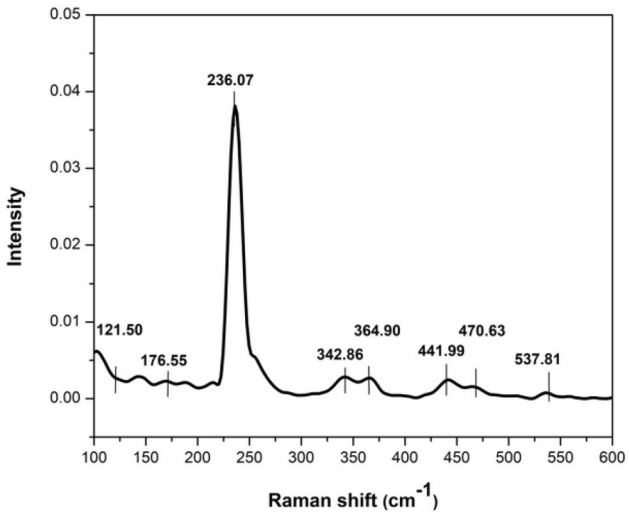

Fig. 8 FT-Raman spectra of synthesized ZnO–ZnSe heterostructures

compared with that of bulk ZnO, ZnSe and $ZnSeO_3$ material [2.7 eV].

3.4 Photoluminescence Analysis

The photoluminescence (PL) spectrum of the synthesized ZnO–ZnSe heterostructures at an excitation wavelength of 300 nm is shown in Fig. 6 with peaks centred around 374,420 and 467 nm. The peaks centered around 3.30 eV (374 nm) and this is due to the electron hole recombination [29]. The weak blue emission centered around 2.94 eV (420 nm) results from recombination of photogenerated hole with charge state specified defects [30] and that centered around 2.65 eV (467 nm) can be ascribed to the NBE of ZnSe (Fig. 7).

3.5 Fourier Transform Raman Spectroscopy (FT-Raman) Analysis

Raman spectroscopy was performed to study the vibrational and electronic properties of the synthesized ZnO/ZnSe heterostructured nanoparticles. Raman peak located at about 121 cm^{-1} (Fig. 8) is caused by the clustering effect as reported by Amirthraj et.al which is quite visible from the SEM images [31, 32]. The interface phonons forms near the hetero-interface of a quantum nanostructure. The peak around 176 cm^{-1} corresponds the E1 mode in wurtzite structure of ZnO/ZnSe [33]. The frequency at 467 cm^{-1} is the E2 mode characteristic of the wurtzite structure of ZnO/ZnSe. The surface phonon mode which is a characteristic feature of nanostructure is seen at 237 cm^{-1} for the

ZnO/ZnSe heretrostructure nanoparticles. All spectra of the ZnSe–ZnO exhibit an absorption peak located at ~ 363 cm^{-1} corresponding to the absorption for bulk ZnO. There is also a weak and broad peak due to the 2nd order phonon mode centered around 500 cm^{-1} [33].

3.6 Photocatalytic Activity

The solar photocatalytic of synthesized nanostructure has been investigated for the degradation of Methylene blue in water. Figure 9 represents the visible light absorption spectra of methylene blue (MB) observed at regular time intervals, with ZnO/ZnSe heterostructures. It was observed that the residual MB dye concentration decreases with increasing visible light exposure time for the sample, which suggest that the synthesized heterostructures using chemical-precipitation method exhibit solar photocatalytic activity. The dye degradation efficiency is calculated based on the following equation [34]

$$\text{Degradation rate} = \left(\frac{C_0 - C}{C_0}\right) \times 100 = \left(\frac{A_0 - A}{A_0}\right) \times 100 \quad (8)$$

Figure 10 represents the degradation rate of methylene blue with time. It is observed that the degradation of the dye decreases with time and almost ceases at 210 min. The maximum degradation corresponds to 66%. The possible reaction mechanism can be as follows. The formation of heterostructures enables charge separation and excess oxygen present facilitates superoxide radical anions and hydroxyl radical formation which causes degradation [7]. The presence of excess oxygen has already been verified by EDX analysis. The absorption spectra are found to remain constant after 150 min. This hindrance in solar photocatalytic activity might be due to the adsorption of methylene blue and also due to the presence of $ZnSeO_3$ which is having a wider bandgap (3.9 eV).

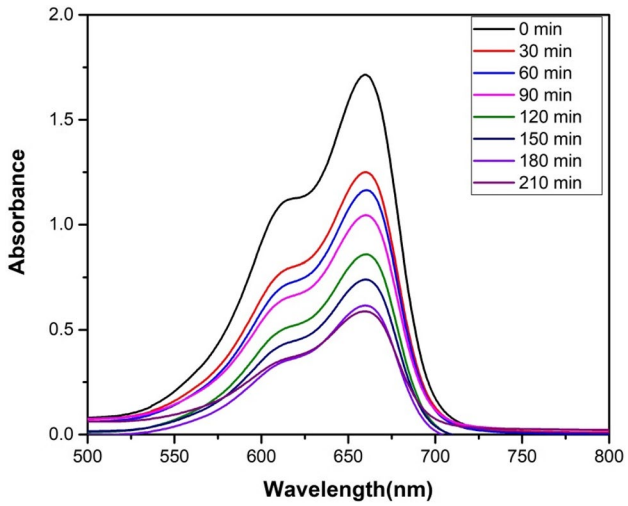

Fig. 9 The visible light absorption spectra of methylene blue (MB) observed at regular time intervals, with the ZnO/ZnSe heterostructures

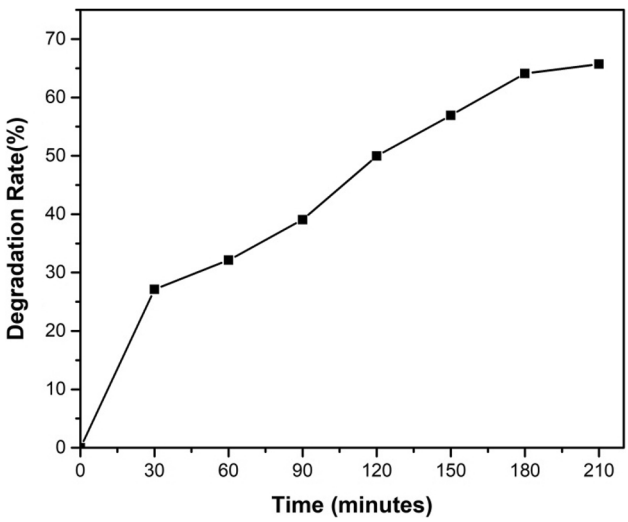

Fig. 10 % degradation of methylene blue (MB) observed at regular time intervals, with the ZnO/ZnSe heterostructures

4 Conclusion

This present work spotlights a simple, cost-effective, environment-friendly single step chemical precipitation approach for the synthesis of single phase ZnO/ZnSe heterostructures. The XRD results confirmed the formation of hexagonal phase of both ZnO and ZnSe nanoparticles. ZnO microspheres grown over the ZnSe nano cauliflower clusters thus forming a ZnO/ZnSe layered plate structure confirming the ZnO/ZnSe heterostructures is been observed from the FESEM images and EDAX results confirms the presence of expected elements in the synthesized nanoparticles. The presence of $ZnSeO_3$ confirmed from the XRD patterns and excess oxygen from EDX pattern is found to have a profound effect in the optical as well as photocatalytic property of the synthesized heterostructures. HRTEM images also confirm the amorphous nature due to single step nucleation. The solar photocatalytic performance of the synthesized ZnO/ZnSe heterostructures has been analysed for methylene blue under visible light and from the results it was observed that ZnO/ZnSe heterostructures catalysts showed improved photocatalytic performance.

Acknowledgements Authors thank Dr. A Karthega and staffs of Biosensor lab in facilitation of experimental part, Karunya University for

XRD measurements, SITRA and CIT, Coimbatore for FESEM and EDAX, STIC, Cochin university for HRTEM analysis, SRMV College Of Arts And Sciences, Coimbatore for giving provision to take UV and PL, and SAIF,IIT Madras for FT-Raman measurements. Authors are also thankful to Mr. Arun Viswan K K, PhD research scholar, Amrita Vishwa Vidyapeetham, Ettimadai, Coimbatore and Dr. Maruthamani of Department of Chemistry, PSG College of Technology, Coimbatore for helping in the application study.

References

1. Y. Wang, Q. Wang, X. Zhan, F. Wang, M. Safdar, J. He, Nanoscale **5**, 8326 (2013)
2. Y. Dong, C. Feng, P. Jiang, G. Wang, K. Li, H. Miao, RSC Adv. **4**, 7340 (2014)
3. W. Zhou, H. Liu, J. Wang, D. Liu, G. Du, J. Cui, A.C.S. Appl, Mater. Interfaces **2**, 2385 (2010)
4. N.M. Rohith, P. Kathirvel, S. Saravanakumar, L. Mohan, Optik (Stuttg). **172**, 940 (2018)
5. Ü. Özgür, Y.I. Alivov, C. Liu, A. Teke, M.A. Reshchikov, S. Do, V. Avrutin, Appl. Phys. Rev. A **98**, 1 (2005)
6. X. Gu, C. Li, S. Yuan, M. Ma, Y. Qiang, J. Zhu, Nanotechnology **27**, 402001 (2016)
7. S. Cho, J. Jang, J.S. Lee, K. Lee, Nanoscale **4**, 2066 (2012)
8. M. Safari, Z. Izadi, J. Jalilian, I. Ahmad, S. Jalali-Asadabadi, Phys. Lett. A **381**, 663 (2017)
9. F.E.N. Qiao, Q. Liang, X. Hou, J. Yang, J. Electron. Mater. **48**, 4418 (2019)
10. P. Chen, L. Gu, X. Cao, CrystEngComm **12**, 3950 (2010)
11. H. Liu, Y. Hu, X. He, H. Jia, X. Liu, B. Xu, J. Alloys Compd. **650**, 633–640 (2015)
12. X. Liu, J. Cao, B. Feng, L. Yang, M. Wei, H. Zhai, Superlattices Microstruct. **83**, 447 (2015)
13. M.F. Ehsan, S. Bashir, S. Hamid, A. Zia, Y. Abbas, K. Umbreen, M.N. Ashiq, A. Shah, Appl. Surf. Sci. **459**, 194 (2018)
14. K. Matras-Postołek, S. Sovinska, A. Węgrzynowicz, Chem. Eng. Process. **135**, 204 (2019)
15. L. Shi-qian, Z. Pei-jiang, Z. Wan-shun, C. Sheng, P. Hong, J. Alloys Compd. **616**, 227 (2014)
16. M.S. Begum, A.J. Ahamed, J. Chem. Pharm. Res. **7**, 2031 (2015)
17. S.D. Hutagalung, S.T. Eng, Z.A. Ahmad, I. Mat, J. Nucl. Relat. Technol. **6**, 147 (2009)
18. M.T. Thein, S. Pung, A. Aziz, M. Itoh, J. Exp. Nanosci. **10**, 1068 (2015)
19. S. Gharibe, S. Afshar, L. Vafay, Bull. Chem. Soc. Ethiop. **28**, 37 (2014)
20. M. Salavati-niasari, F. Davar, M. Mazaheri, Mater. Lett. **62**, 1890 (2008)
21. K. Ravichandran, S. Snega, N.J. Begum, L. Rene, Philos. Mag. **94**, 37 (2014)
22. Z. Selenite, https://materialsproject.org/materials/mp-5338/ (n.d.).
23. P. Zhang, C. Shao, X. Li, M. Zhang, X. Zhang, Y. Sun, Y. Liu, J. Hazard. Mater. **237–238**, 331 (2012)
24. R. Yousefi, M.R. Muhamad, A.K. Zak, Thin Solid Films **518**, 5971 (2010)
25. S.A. Hassan, S. Bashir, K. Zehra, Q.S. Ahmed, Mater Res Express **5**, 046404 (2018)
26. C. Aydn, M. Abdel-sadek, K. Zheng, I.S. Yahia, F. Yakuphanoğlu, Opt. Laser Technol. **48**, 447 (2013)
27. A. Narmada, P. Kathirvel, L. Mohan, S. Saravanakumar, R. Marnadu, J. Chandrasekaran, Opt. Int. J. Light Electron Opt. **202**, 163701 (2020)
28. Z.K. Heiba, K. El-sayed, Egypt. J. Sol **23**, 37 (2000)
29. H. Li, B. Wang, L. Li, J. Alloys Compd. **506**, 327 (2010)
30. K. Senthilkumar, T. Kalaivani, S. Kanagesan, V. Balasubramanian, J. Mater. Sci. Lett. **23**, 2048 (2012)
31. K.K. Tiong, P.M. Amirtharaj, P. Parayanthal, F.H. Pollak, Solid State Commun. **50**, 891 (1984)
32. P.M. Amirtharaj, K. Tiong, F.H. Pollak, J. Vaccum Sci. Technol. **1744**, 1 (2014)
33. P. Iranmanesha, S. Saeedniab, M. Nourzpoora, Chin. Phys. B **24**, 046104 (2015)
34. K. Saeed, I. Khan, T. Gul, M. Sadiq, Appl. Water Sci **7**, 3841 (2017)